Annals of Biomedical Engineering, Vol. 33, No. 2, February 2005 (©2005) pp. 150–164
DOI: 10.1007/s10439-005-8974-7

Study of Ocular Transport of Drugs Released from an Intravitreal Implant Using Magnetic Resonance Imaging

HYUNCHEOL KIM,[1] MARTIN J. LIZAK,[2] GINGER TANSEY,[3] KARL G. CSAKY,[3] MICHAEL R. ROBINSON,[3] PENG YUAN,[4] NAM SUN WANG,[5] and ROBERT J. LUTZ[1]

[1]Divison of Bioengineering and Physical Science ORS, National Institutes of Health, Bethesda, MD 20892; [2]National Institute of Neurological Disease and Stroke, National Institutes of Health, Bethesda, MD 20892; [3]National Eye Institute, National Institutes of Health, Bethesda, MD 20892; [4]Pharmacy Department, National Institutes of Health, Bethesda, MD 20892; and [5]Department of Chemical Engineering and Bioengineering Program, University of Maryland, College Park, MD 20742

(Received 4 February 2004; accepted 26 August 2004)

Abstract—Ensuring optimum delivery of therapeutic agents in the eye requires detailed information about the transport mechanisms and elimination pathways available. This knowledge can guide the development of new drug delivery devices. In this study, we investigated the movement of a drug surrogate, Gd-DTPA (Magnevist®) released from a polymer-based implant in rabbit vitreous using T_1-weighted magnetic resonance imaging (MRI). Intensity values in the MRI data were converted to concentration by comparison with calibration samples. Concentration profiles approaching pseudosteady state showed gradients from the implant toward the retinal surface, suggesting that diffusion was occurring into the retinal–choroidal–scleral (RCS) membrane. Gd-DTPA concentration varied from high values near the implant to lower values distal to the implant. Such regional concentration differences throughout the vitreous may have clinical significance when attempting to treat ubiquitous eye diseases using a single positional implant. We developed a finite element mathematical model of the rabbit eye and compared the MRI experimental concentration data with simulation concentration profiles. The model utilized a diffusion coefficient of Gd-DTPA in the vitreous of 2.8×10^{-6} cm^2 s^{-1} and yielded a diffusion coefficient for Gd-DTPA through the simulated composite posterior membrane (representing the retina–choroid–sclera membrane) of 6.0×10^{-8} cm^2 s^{-1}. Since the model membrane was 0.03-cm thick, this resulted in an effective membrane permeability of 2.0×10^{-6} cm s^{-1}. Convective movement of Gd-DTPA was shown to have minimal effect on the concentration profiles since the Peclet number was 0.09 for this system.

Keywords—T_1-weighted magnetic resonance imaging, PVA-based implant, Gd-DTPA, Finite element eye model, Ocular drug delivery.

INTRODUCTION

Diseases affecting the posterior segment of the eye, age-related macular degeneration (AMD), and diabetic retinopathy are the main causes of blindness in developed countries. Topical administration such as eye drops accounts for nearly 90% of the currently accessible market formulations.[6] However, less than 5% of topically applied therapeutic agent passes through the cornea because of tear flow drainage, dilution by blinking, corneal diffusion resistance, and aqueous humor washout.[6,16,39] Systemic administration of biologically active agents often fails to deliver to some target sites at therapeutic levels because of the blood–retina barrier and the blood–aqueous barrier.[10] For effective treatment, large systemic doses are often required, which can cause systemic adverse effects. Intravitreal injection is a current method being used to deliver drugs directly to the posterior segment of the eye.[21,44] However, since many ocular drugs have narrow therapeutic ranges[32] and are eliminated rapidly from the vitreous,[40] special caution is required to keep a therapeutic level in the vitreous without adverse effects. In addition, many posterior ocular diseases are chronic, requiring repeated injections, which may give patients discomfort, and potentially cause retinal detachment, hemorrhage, or endophthalmitis.[24,36] To overcome the limitations of delivering drugs to the eye by topical administration, systemic injection, and intravitreal injection, interest has increased in the use of sustained release delivery methods.[2,6,11,31,42] Well known is the intravitreal ganciclovir implant (Vitrasert, Bausch & Lomb) for treating cytomegalovirus retinitis in AIDS.[9]

The distribution of injected materials in the vitreous has been studied theoretically and experimentally[13,34,41] and the movement of drugs released from an implant in the vitreous has been studied theoretically.[28,37,39] These studies did not correlate these simulations with real-time data on the distribution and elimination of drugs released from intravitreal implants. In view of the increased interest in sustained

Address correspondence to Dr. Robert J. Lutz, Drug Delivery and Kinetics Resource, Division of Bioengineering and Physical Science ORS, Building 13, Room 3N17, 9000 Rockville Pike, Bethesda, MD 20892. Electronic mail: rjlutz@mail.nih.gov

Abbreviations used: Gd-DTPA, gadolinium-diethylenetriaminopentaacetic acid; PVA, polyvinyl alcohol; TR, repetition time; TE, echo time; FOV, field of view; RCS, retina–choroid–sclera; PBS, phosphate buffered saline.

release methods, more information is needed on the movement of drugs released from an implant in the eye since this knowledge is crucial for developing improved drug delivery systems.

Magnetic resonance imaging (MRI) has been utilized to investigate the anatomy and pathology of the eye noninvasively.[3,7,17,23] In this study, we employed MRI to overcome limitations in autoradiography and fluorescence, which do not yield real-time information and require tedious dissection procedures. We determined noninvasively the real-time movement of a drug surrogate, gadolinium-diethylenetriaminopentaacetic acid (Gd-DTPA) released from a polymer-based intravitreal implant. To help analyze the MRI experimental data, we also developed a finite element mathematical eye model.

METHODS

Intravitreal Implant Design

Intravitreal implants were manufactured as follows (Fig. 1): 15% (w/v) polyvinyl alcohol (PVA) solution was formulated by placing 1.5 g of PVA (Airvol 125, 99.48 mol% hydrolysis, Air Products and Chemicals, Allentown, PA) in 10 ml of molecular biology grade water (BIOfluids®, Biosource International, Camarillo, CA) in a 50-ml polypropylene conical tube (Falcon®, BD Biosciences, Franklin Lakes, NJ) and placed in a water bath at 100°C for 3 h to dissolve all the PVA. After the PVA solution was cooled to room temperature, 0.80 ml of 0.5 M gadolinium-diethylenetriaminopentaacetic acid (Gd-DTPA) (MW = 938) solution (Magnevist®, Berlex, Richmond, CA) was added and stirred into the PVA mixture to produce a 15% PVA and 20% Gd-DTPA (w/w/v) solution. A portion of the solution was poured onto a glass plate, which produced a thin film as it dried at room temperature.

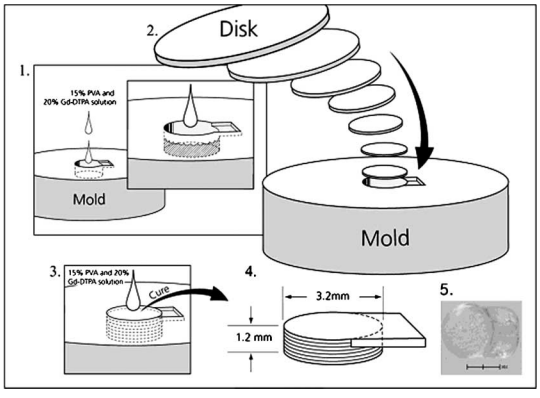

FIGURE 1. Fabrication procedure for the intravitreal implant. 1: PVA/Gd-DTPA solution in mold. 2: PVA/Gd-DTPA dry matrix discs inserted. 3: Complex cured. 4: Schematic of implant removed from the mold with dimensions. 5: Photograph of the Gd-DTPA intravitreal implant.

Disks were made with a biopsy punch (Acu·Punch®, 3 mm, Acuderm, USA) to make 3-mm diameter disks. Individual disks were placed in a Teflon mold, which had a 3.4-mm diameter bore of 1.2-mm depth. The disks were coated with the remaining 15% PVA & 20% Gd-DTPA (w/w/v) solution. The dried implant was peeled out of the Teflon mold. These 3.4-mm diameter by 1.2-mm thick implants were suitably sized for insertion in the vitreous cavity of a rabbit's eye.

In Vitro Release Rate

In vitro release rate experiments were performed on the fabricated implants over an 8-h period, which was equivalent to the MRI experimental time period. In one study, test implants were placed in 25-ml glass vials with 20 ml of phosphate buffered saline (PBS) (pH 7.4) and stirred at 150 rpm at room temperature. The solution was assayed every 10 min for the first hour, every 30 min for the second hour, and then hourly up to 8 h. The PBS solution was completely replaced with fresh PBS at each sample time to provide a sink condition. Gd-DTPA concentrations in the sampled solutions were measured on a spectrofluorometer (QuantaMaster, Photon Technology International, Lawrenceville, NJ), after calibration with known Gd-DPTA concentrations, at excitation wavelength 275 nm and emission wavelength 312 nm. The release rates were determined by calculating the amount of Gd-DTPA released over time and recorded as milligram per hour. The *in vitro* release rate assays were also carried out in unstirred liquids to more closely simulate *in vivo* conditions. Both unstirred PBS and an unstirred viscous liquid of 2% hydropropyl methylcellulose (HPMC) (METHOCEL®, Dow Chemical) were used. These solutions were not replaced after each assay time, but rather, a series of reservoirs were set up at the same start time and sampled sequentially at various sample times.

Magnetic Resonance Imaging

Standard Solutions for Quantitative Analysis of MRI Images

To compare successive MRI images from day to day and to calibrate the amount of Gd-DTPA in the vitreous and in the aqueous humor, standard solutions of known Gd-DTPA concentration were always scanned along side the rabbit eyes. The standard solutions were prepared by adding varying amounts of 0.5-M Gd-DTPA solution to 2% HPMC solution[33] to make 1.0×10^{-1}, 0.5×10^{-1}, 1.0×10^{-2}, 0.5×10^{-2}, 0.25×10^{-2}, 1.0×10^{-3}, 0.5×10^{-3}, 1.0×10^{-4}, 0.5×10^{-4}, 1.0×10^{-5}, 0.5×10^{-5}, and 1.0×10^{-6} M calibration solutions. Each of the 12 calibration solutions was sealed with silicone into 12 individual wells cut from a standard 96-well plate culture chamber (VWR international, Bridgeport, NJ). Gray scale images

of the standard solutions were developed and the average intensity value of each concentration was determined using ImageJ software (version 1.27z, National Institutes of Health, Bethesda, USA). A calibration curve of image intensity versus Gd-DTPA concentration was generated.

In Vivo Experiment

All imaging experiments were performed *ex vivo* and *in vivo* on New Zealand White rabbits in a 4.7-Tesla magnet equipped with a Bruker Avance console (Brukerbiospin, Billerica, MA). The procedures adhered to the guidelines from the *PHS Guide for Care and Use of Laboratory Animals*. All analyses and manipulations of images were performed using MATLAB (version 6.5, Mathworks Inc., Natick, MA) and AMIRA (version 2.3, TGS Inc., San Diego, CA).

Each rabbit was maintained under general anesthesia during the entire imaging period. The animals were induced with xylazine (5–10 mg kg^{-1}) and ketamine (35–50 mg kg^{-1} IM to effect) and an IV catheter was inserted into the marginal ear vein to administer fluids. An endotracheal tube was placed and anesthesia was maintained with 1–2% halothane or 1–2% isoflurane. The conjunctiva was opened approximately 5 mm posterior from the limbus. The exposed sclera was opened with a stab incision (using a Beaver blade), and an intravitreal implant was placed into the vitreous chamber. The implant was sutured to the sclera; the sclera and conjunctiva were closed with suture. After completing this preparation, the rabbit was positioned in the MRI. T_1-weighted MRI studies were performed using a 10-cm diameter volume coil and a Fast Spin Echo sequence. MRI scanning parameters were TR/TE = 200/9.0 ms, with a 9 cm × 9 cm × 9 cm field of view (FOV), and a 256 × 128 × 128 acquisition matrix size for the *in vivo* experiment. A complete 3D data set was acquired every 20 min. During the study, pulse, blood oxygenation (SpO_2), end-tidal CO_2, respiratory rate, anesthetic gas levels, and body temperature were monitored.

Ex Vivo Experiment

Eyes were enucleated from euthanasized rabbits. The conjunctiva was opened approximately 5 mm posterior from the limbus. The exposed sclera was opened with a stab incision (using a Beaver blade), and an intravitreal implant was placed into the vitreous chamber. The implant was sutured to the sclera; the sclera and conjunctiva were closed with suture. After placing the implant in the vitreous, the eye was placed in a 50-ml centrifugal tube, on a wet (sterile saline) sterile 4 in. × 4 in. gauze pad, to keep the eye moisturized. After completing this preparation, the tube was immediately positioned in the MRI. The eye was scanned every 10 min for 20 h using a 72-mm diameter volume coil and a Fast Spin Echo sequence. MRI scanning parameters were TR/TE = 200/6.6 ms, FOV = 5 cm × 5 cm × 4 cm, echo train length = 8 ms, 256 × 128 × 128 acquisition matrix size, and 2 averages.

3D Computer Simulation

A 3D finite element mathematical model of the eye was developed using FEMLAB software (version 3.0, Consol Inc., Burlington, MA) to help analyze MRI images and to assist our understanding of the transport of Gd-DTPA released from an intravitreal implant. The geometry of the mathematical model of the eye was based on the physiological dimensions of a rabbit eye[20] and was composed of vitreous, lens, a hyloid surface, a posterior membrane, and an implant [Fig. 2(A)]. In this initial model, the posterior surface is described as a "lumped" homogeneous membrane region that represents the combined retina–choroid–sclera barrier, henceforth referred to as the RCS region. The actual

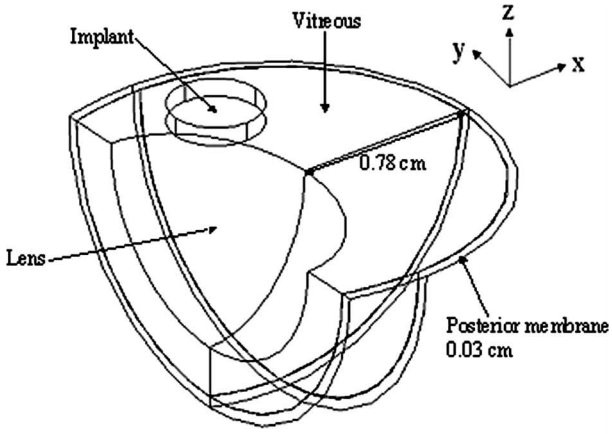

(A)

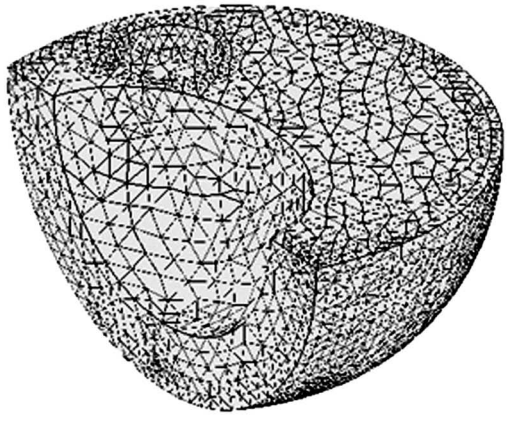

(B)

FIGURE 2. (A) The geometry and dimensions of finite element with implant. (B) meshed eye model with 3958 nodes.

TABLE 1. Parameter values used in the simulation study.

Parameter	Value	Reference
Viscosity of aqueous humor	6.9×10^{-3} g cm^{-1} s^{-1}	Friedrich *et al.*[13]
Pressure at the hyaloid	15 mmHg	Missel[28]
Pressure at the episclera	10 mmHg	Missel[28]
Hydraulic conductivity in the sclera	1.5×10^{-11} cm^2 Pa^{-1} s^{-1}	Xu *et al.*[43]
Hydraulic conductivity in the vitreous	2.4×10^{-6} cm^2 Pa^{-1} s^{-1}	Xu *et al.*[43]
Diffusivity of Gd-DTPA in the vitreous	2.8×10^{-6} cm^2 s^{-1}	Gordon *et al.*[38] and confirmed by our *ex vivo*
Diffusivity of Gd-DTPA through the posterior membrane	6.0×10^{-8} cm^2 s^{-1}	Estimated from this study
Permeability of Gd-DTPA in the posterior membrane	2.0×10^{-6} cm s^{-1}	Calculated from membrane diffusivity and membrane thickness = 0.03 cm

posterior membrane is structurally more complex than this model simplification. It consists of multiple layers of tissue and an array of blood vessels. Our initial approach to model this barrier is somewhat simplistic at this time and further refinements can be done in future work. Using the "lumped" posterior membrane in the model allows us to make reasonable simulations of the vitreous concentration data. There is not sufficient explicit data to warrant a more complex representation at this time. The finite element mesh that was used by FEMLAB contained 3958 nodes [Fig. 2(B)].

To determine the velocity distribution of the fluid movement through the eye, Darcy's law was applied to the vitreous compartment and to the posterior membrane[43]:

$$\vec{U} = -\frac{K}{\mu}\nabla p \tag{1}$$

where, $\vec{U}$ is the velocity of the fluid, K is the hydraulic conductivity of the vitreous or posterior membrane, μ is the viscosity of the fluid, and ∇p is the pressure gradient. Values of the hydraulic conductivity for vitreous gel and for the RCS membrane and a value of the viscosity of the aqueous fluid were derived from the literature (see Table 1). Pressures of 15 mmHg and 10 mmHg were applied to the hyaloid and the outer sclera, respectively, to achieve a 5-mmHg pressure drop between these elements.[14] The lens and the implant were considered to be impermeable to fluid flow, so, a zero velocity fluid flow boundary condition was applied throughout the lens and the implant. To calculate the concentration distribution of the released Gd-DTPA in the vitreous region, the following diffusion-convection equation was solved[28]:

$$\frac{dC}{dt} - \nabla\cdot(D\nabla C) + \vec{U}\cdot\nabla C = 0, \tag{2}$$

where, D is the diffusion coefficient of Gd-DTPA in the vitreous, $\vec{U}$ is the velocity of fluid in the vitreous, and C is the concentration of Gd-DTPA. To expedite the computation time, the steady state vitreous velocity distribution of the fluid was first calculated from the Darcy's law equation and that velocity vector field was exported into and superimposed on the diffusion-convection equation to determine concentration distribution of Gd-DTPA in the vitreous.

A mass flux boundary condition was imposed on the surface of implant to simulate the measured *in vitro* release rate data. The rate and time course of the release in the simulations, determined from the *in vitro* release data, is depicted in Fig. 3.

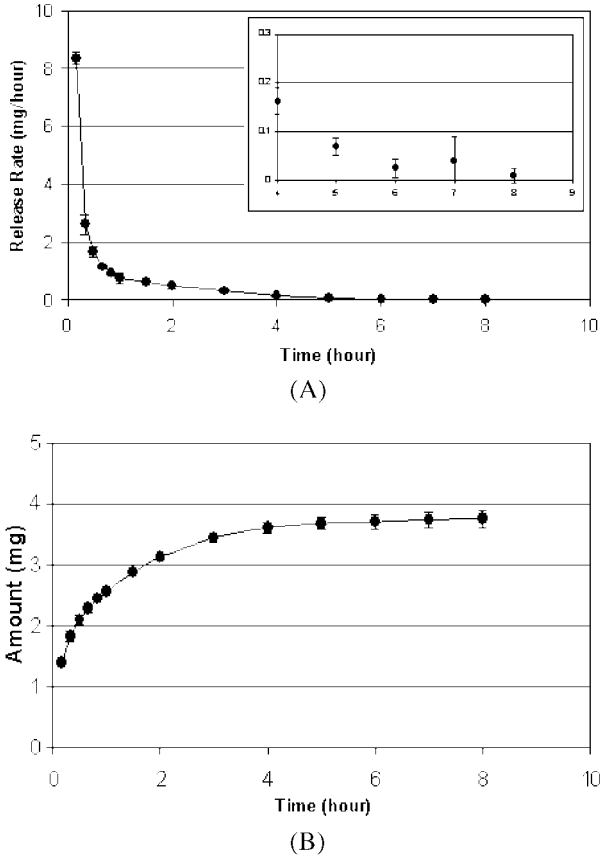

FIGURE 3. (A) *In vitro* release rate of Gd-DTPA from intravitreal implants. Insert has expanded concentration scale from 4 to 8 h; (B) cumulative amount of released Gd-DTPA. The implant was loaded initially with 4.0 mg of Gd-DTPA.

At the outer boundary of our lumped posterior membrane, a zero concentration boundary condition was applied. This condition could represent a rapid "sink" condition within some region of the membrane layers, possibly as rapid clearance by choroidal blood flow, resulting in a near zero concentration in the outermost sclera layer. This assumption is further substantiated by additional data that we have collected (paper accepted for publication, IVOS) which compares *in vitro* and *ex vivo* transport of Gd-DPTA from an episcleral implant and by published work by Missel[29] who describes several viable mathematical representations of the posterior membrane and its relevant boundary conditions. Regarding the MRI experiments using episcleral positioning of the implant, we observed that, during an *in vivo* experiment, only negligible amounts of Gd-DPTA were ever detected in the vitreous fluid. However, during an *ex vivo* experiment with an episcleral implant sutured to an explanted eye, significant amounts of Gd-DPTA were observed to accumulate in the vitreous over time. One possible explanation, and our reasoning for the zero concentration boundary condition assumption, was that the choroid acted as a "complete" sink for the small molecular weight Gd-DPTA, allowing negligible amounts to cross. That observation could suggest that this "sink" would also operate during Gd-DPTA movement from the vitreous side toward the sclera with essentially no Gd-DPTA reaching the scleral layer. Missel[29] defines a "gamma" term as the ratio of the concentration at the sclera to the concentration at the retina–choroid interface. If we relate the "sink" term in the Missel analysis to the choroidal blood flow per unit tissue volume (we estimate 0.21 s^{-1}), we would estimate a gamma of 0.01 based on Missel's analysis (Ref. 29, Fig. 3). We have set this value to zero in our model as the concentration boundary condition at the outer surface of our lumped posterior membrane.

A continuity condition was applied at the interface between the vitreous and posterior membrane of the eye both in the flow velocity calculation and in the diffusion-convection calculation. The current model does not include an anterior eye segment (e.g. cornea, iris, and aqueous chamber). Instead, in order to account for the loss of drug to the anterior segment, a boundary condition was used at the hyaloid membrane that represented drug clearance to the anterior region, similar to the procedure used by Missel.[28] The clearance was represented in the model as a flux boundary condition at the hyaloid membrane which was calculated as the aqueous humor turnover rate divided by the hyaloid area times the hyaloid drug concentration at each time point:

$$\text{Flux of drug} = -(f \times A^{-1}) \times C$$

where f is the turnover rate of aqueous humor (3.7×10^{-11} m^3 s^{-1}), A is the hyaloid area (6.0×10^{-5} m^2), and C is the concentration at the hyaloid membrane. The Gd-DTPA flux value equaled -6.16×10^{-5} [cm s^{-1}] $\times C$. Other parameter values that were used for the mathematical eye model are listed in Table 1.

Quantitative comparisons between simulations and the MRI concentration data were made on a relative basis, using the concentration value at the lens-vitreous interface as the normalizing value. Also, the MRI concentration profiles for any given *X–Y* plane in the vitreous space were actually averaged over several adjacent "*Z*" layers in order to smooth out any irregularities that may occur in the vitreous material. The averaged image slices were taken near the global equator of the eye. The simulation concentration profiles, which were compared to the MRI data, were similarly averaged over the same virtual thickness as the MRI slice.

RESULTS

In Vitro Release Rate

Figure 3(A) shows the results of the study of the *in vitro* release rate of Gd-DTPA from the PVA matrix implants in a stirred aqueous buffer. Similar implants were used in both *ex vivo* and *in vivo* experiments. The release rate was initially high followed by a slow decrease with time for up to 8 h. The initial rapid release is typical of matrix type implants.[19] Figure 3(B) shows accumulated amount of Gd-DTPA released from the implants in this *in vitro* system.

The release rates for the unstirred systems of either buffer or the viscous gel (METHOCEL) were, for all practical purposes, the same quantitatively and qualitatively as shown in Fig. 3. The release of Gd-DPTA from the PVA implant appears to be rate controlled within the polymer matrix.

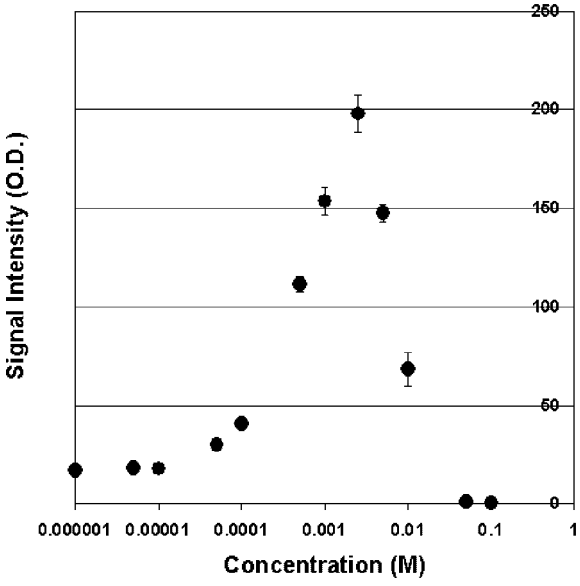

FIGURE 4. The relationship between standardized concentrations of Gd-DTPA in 2% HPMC and signal intensity (in optical density units, O.D.) obtaining during an *in vivo* MRI experiment. Bars represent standard deviations.

Calibration of MRI Images with Gd-DTPA Concentration

The relationships between the concentration of Gd-DTPA in 2% HPMC and image intensity values were determined during each MRI experiment to account for daily variations in the instrument setup which may affect absolute intensity measurements. Figure 4 shows a typical relationship between Gd-DTPA concentration and image intensity in standardized HPMC calibration solutions obtained during an *in vivo* experiment. The intensity signal initially increased with increasing concentration of Gd-DTPA up to 0.5×10^{-2} M. Above 0.5×10^{-2} M, the intensity signal decreased with Gd-DTPA concentration because of T_2 shortening effects. Image intensity variation with Gd-DTPA concentration was indistinguishable below 0.5×10^{-5} M Gd-DTPA so that any measured concentrations of Gd-DTPA below 0.5×10^{-5} M were set to zero. The calibration results show that the range of Gd-DTPA concentrations for useful analysis was nearly 3 decades of variation from approximately 0.5×10^{-5} to 0.5×10^{-2} M.

MRI Images

In Vivo

Figure 5 shows the MRI intensity images in a rabbit eye at 1.5, 2.7, 4.1, and 7.7 h following insertion of an intravitreal Gd-DTPA implant ($n = 4$). The dark rectangle outlines the implant location and appears black due to the saturation T_2 effects of the high Gd-DTPA concentration in the implant. The large oval-shaped dark region to the lower right of the implant is the rabbit lens which is impermeable to the Gd-DTPA and presents black due to insignificant concentration in the lens. Gd-DTPA can be seen to disperse through large regions of the vitreous compartment as time progresses. There is a definite concentration gradient from

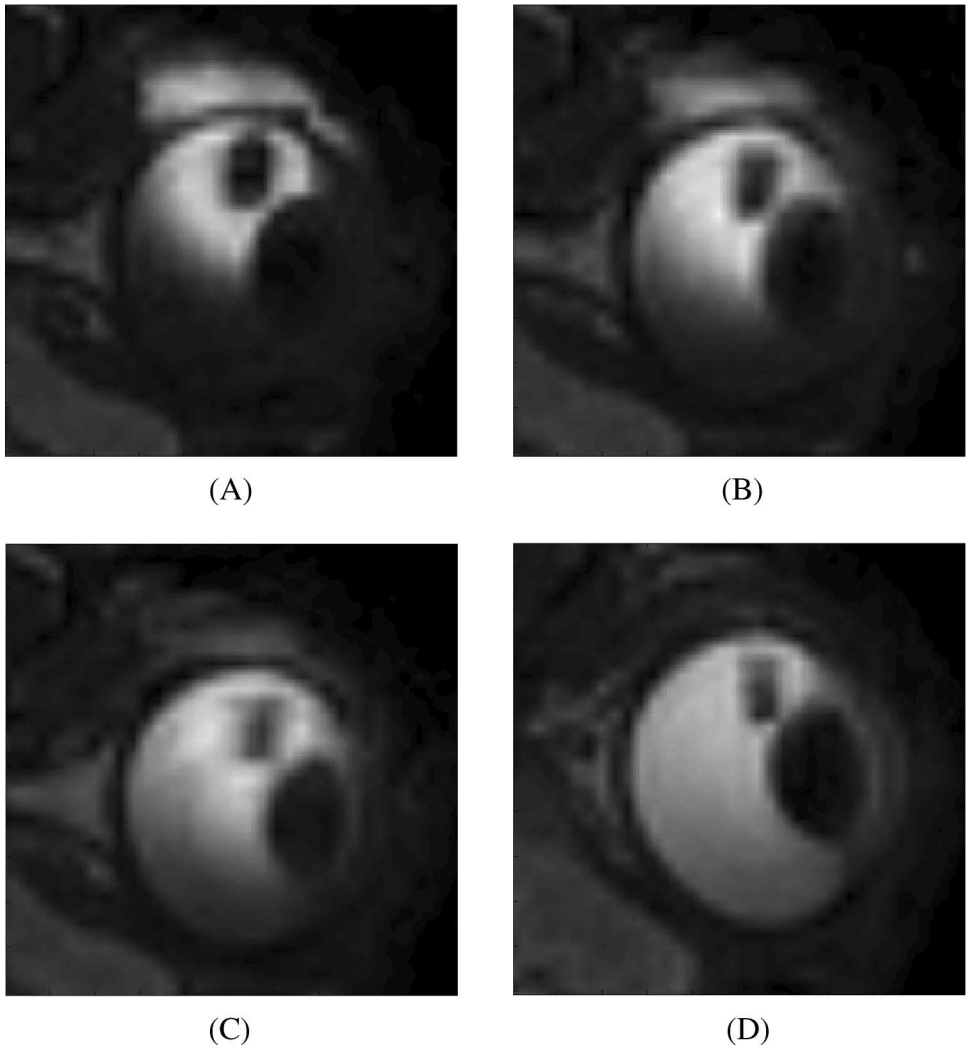

FIGURE 5. ***In vivo*** **MR images of Gd-DTPA in rabbit eyes at various times post-implantation from intravitreal implant: (A) 1.5 h, (B) 2.7 h, (C) 4.1 h, and (D) 7.7 h.**

high to low concentration as one proceeds from a near implant to a distant position in the vitreous. A more detailed analysis of the concentration profiles is presented in a later section, but a distinct concentration gradient is maintained with the *in vivo* system up to nearly 8-h post-implantation. Some Gd-DTPA was evident at the incision site which may have occurred by implant contact with moist tissue during insertion or by some leakage or diffusion of Gd-DTPA back to the incision area. Very little signal intensity is seen in the anterior chamber of the *in vivo* eye of Fig. 5. Also, a dark ring is observed around the posterior segments of the eye in an area of the RCS membrane, which may represent an undetectable, low Gd-DTPA concentration.

Ex Vivo

Figure 6 shows the MRI images in an *ex vivo* rabbit eye at 1.2-, 2.6-, 4.6-, and 10.1-h postimplantation. These images show more spatial resolution near the eye since a smaller surface coil was placed closer to the eye during these *ex vivo* experiments. The Gd-DTPA implant is clearly visible as the thin rectangular dark region. Gd-DTPA was not detected in the lens, which remains dark. The Gd-DTPA is seen to diffuse in both anterior (toward the aqueous chamber) and posterior (toward the retina) directions. Gd-DTPA begins to diffuse through the hyaloid membrane and accumulate in the aqueous chamber, since there is no clearance by aqueous outflow in the *ex vivo* eye. This situation is a contrast to the *in vivo* case. At 10.1 h, the image intensity within the implant actually appears to brighten since the implant's Gd-DTPA concentration is diminishing below the saturation values (black image). The image intensity at 10.1 h shows a substantially more uniform concentration distribution from the back of the lens toward the retina with essentially no gradient as one proceeds distal to the implant. This *ex vivo* distribution represents a distinct contrast to the *in vivo* data and most likely occurs due to the lack of transport of Gd-DTPA through the RCS layer in the *ex vivo* eye.

Figures 7(A) and 7(B) show the time course of the *in vivo* and *ex vivo* profiles of Gd-DTPA concentration calculated

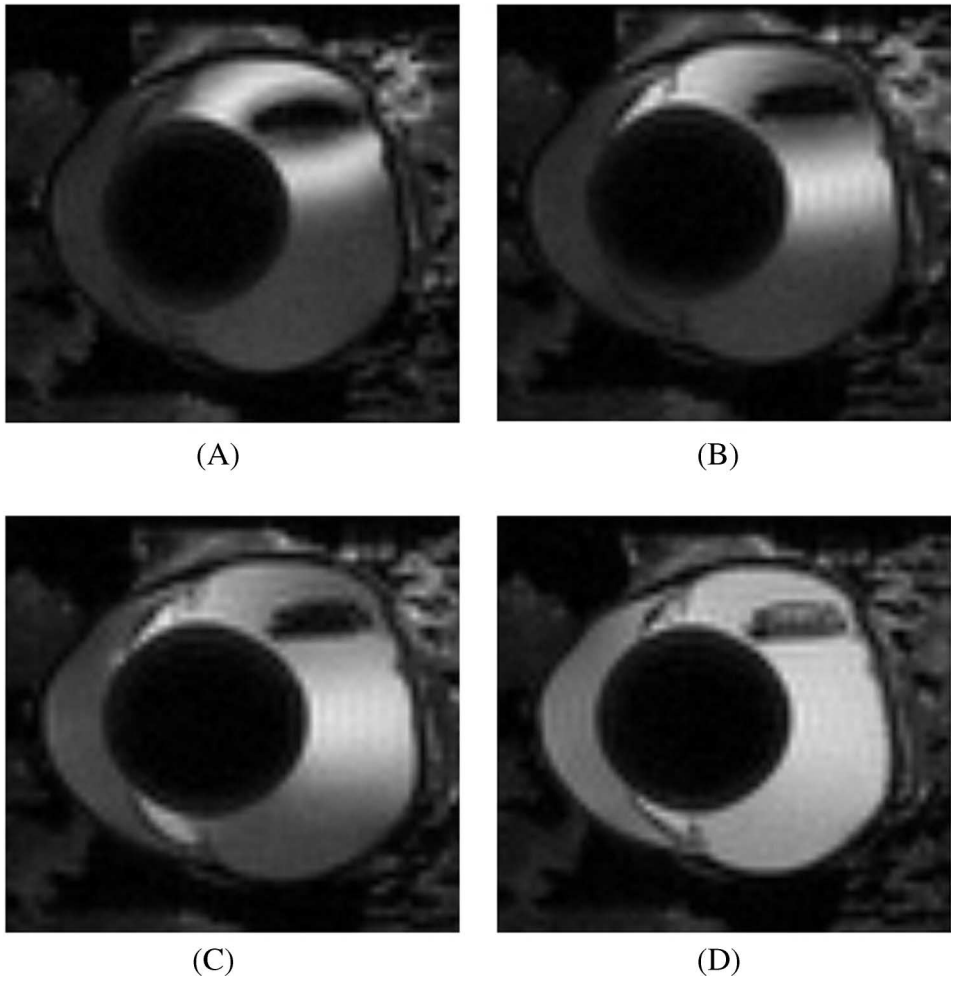

FIGURE 6. *Ex vivo* MR images of Gd-DTPA in rabbit eyes at various times postimplantation from intravitreal implant: (A) 1.2 h, (B) 2.6 h, (C) 4.6 h, and (D) 10.1 h.

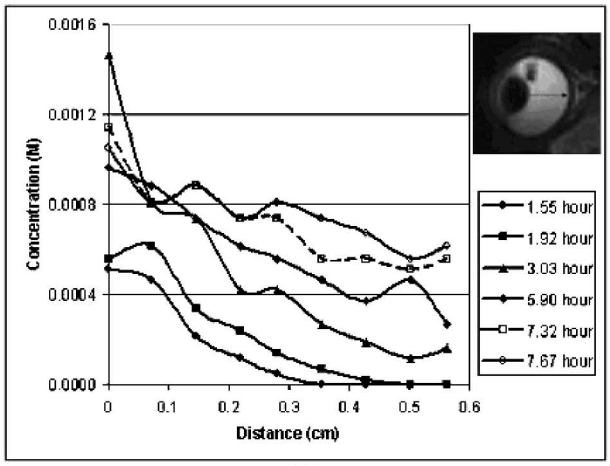

(A)

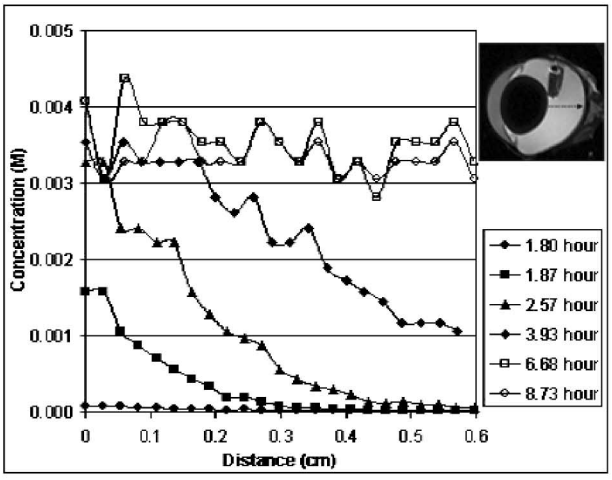

(B)

FIGURE 7. Concentration distribution of Gd-DTPA from the lens to the retina calculated along the line marked by the arrow in the image insert: (A) *in vivo* MRI experiment and (B) *ex vivo* MRI experiment.

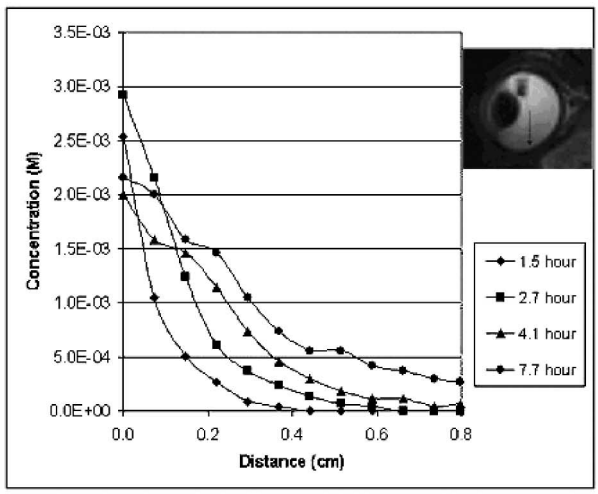

(A)

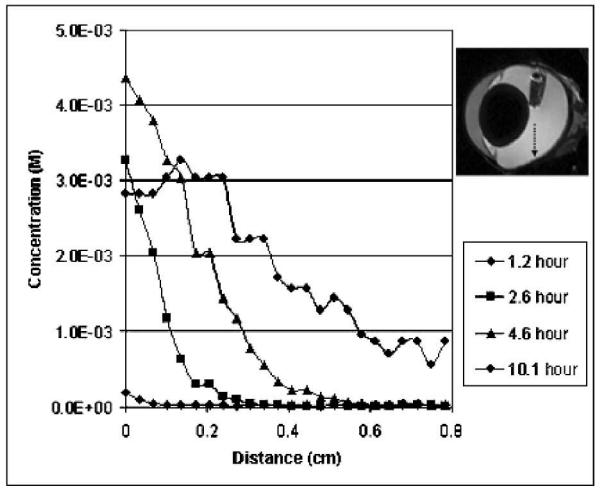

(B)

FIGURE 8. Concentration distribution of Gd-DTPA within the vitreous in a vertical direction away from the implant marked by the arrow in the image insert: (A) *in vivo* MRI experimental data and (B) *ex vivo* MRI experimental data.

from the intensity images along a line drawn from the lens to the retina. For the *in vivo* case, the concentration profile for Gd-DTPA from the lens to the retina appears to approach a "quasi steady state" by about 7.32-h postimplantation and there is a persisting concentration gradient toward the posterior surface. For the *ex vivo* experiment, the concentration profile becomes relatively flat by 6.68 h and remains without a gradient from that time on.

Figures 8(A) and 8(B) show MRI experimental Gd-DTPA concentration profiles taken along the vertical arrow from the middle of the vitreous to a point opposite the implant in the *in vivo* case and *ex vivo* case, respectively. Figure 8(A) shows the concentration values at different time points along this vertical axis for the *in vivo* case. At the longest experimental time point of 7.7 h, there is still a significant drop in Gd-DTPA concentration from the implant side of the vitreous compartment (tail of the arrow represents 0.0 cm on the *x*-axis) to the far side (head of the arrow represents 0.8 cm on the *x*-axis). A similar situation exits for the *ex vivo* case, as shown in Fig. 8(B), except that by 10.1 h, the concentration on the far side (0.8 cm) is finally beginning to rise somewhat as the Gd-DTPA will eventually approach a uniform concentration throughout the *ex vivo* eye.

3D Computer Simulation

From the mathematical eye model, the velocity distribution of the fluid convection in the vitreous compartment was calculated. Figure 9 shows a steady state, gray scale velocity contour with arrows marking velocity directions. The fluid flows from the hyaloid membrane toward

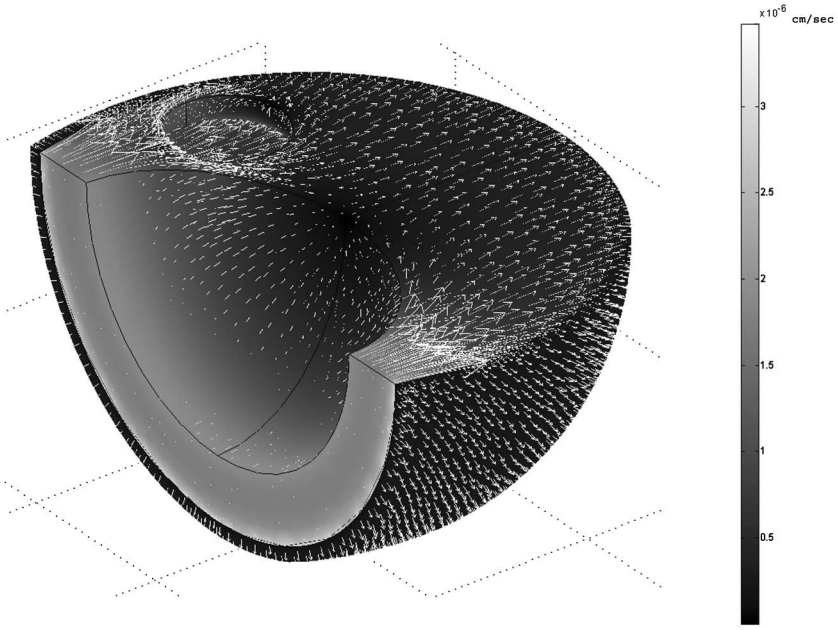

FIGURE 9. Finite element model results of the aqueous humor flow velocity vectors at steady state.

and then out through the RCS membrane. The average velocity through the posterior surface was approximately 3.52×10^{-7} cm s^{-1}. This velocity compares favorably to the value of 3.5×10^{-7} cm s^{-1} found by Missel[20] and 3.9×10^{-7} cm s^{-1} by Araie[1] near the optic nerve. Flow from the ciliary body toward the anterior compartment was not explicitly included in this version of the model. Instead, a clearance term consisting of aqueous humor turnover divided by hyaloid area was used to describe movement of Gd-DTPA to the anterior compartment as described in the Methods section.

The diffusion coefficient for Gd-DPTA in vitreous for the model simulations was set at 2.8×10^{-6} cm^2 s^{-1} according to Gordon *et al.*[18] We confirmed the appropriateness of this diffusivity value by comparing model simulations of the vitreous concentration profiles with experimental data for the *ex vivo* situation. In such a case, the diffusion of Gd-DPTA alone was the sole transport mechanism, with no convective flow or permeation across the *ex vivo* posterior membrane to affect the concentration profiles. Figure 10 shows the comparisons of the simulation of vitreous concentration profiles with the MRI data for the *ex vivo* case when using 2.8×10^{-6} cm^2 s^{-1} as the diffusion coefficient. The inserted MR image in Fig. 10 designates the three locations within the vitreous space where the profiles were taken, corresponding to the three curves. Since this choice of vitreous diffusion coefficient appears to give reasonable results, we then varied the model value of the diffusion coefficient for the "lumped" posterior membrane to obtain the best fit by least squares regression between the *in vivo* MRI vitreous concentration profiles and the *in vivo* model simulations. The posterior membrane was assigned a thickness of 0.03 cm, so setting the diffusion coefficient is tantamount to establishing an "effective" permeability coefficient through the posterior membrane (diffusion coefficient divided by membrane thickness).

Our resulting model vitreous concentration profiles are depicted in Figs. 11(A)–11(D). They show the surface plots of the concentration distribution of Gd-DTPA in the vitreous at several time points. Qualitatively, the model shows a time course and pattern of drug dispersion similar to the MRI *in vivo* images.

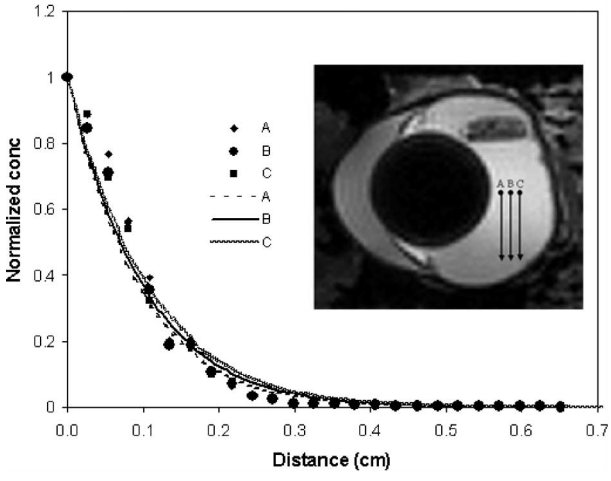

FIGURE 10. (A) Normalized concentration profiles along several vertical location in an *ex vivo* rabbit eye. Points represent MR data and lines represent the corresponding model simulation using 2.8×10^{-6} cm^2 s^{-1} as the Gd-DTPA diffusion coefficient in the vitreous. (B) indicates the location of concentration comparison.

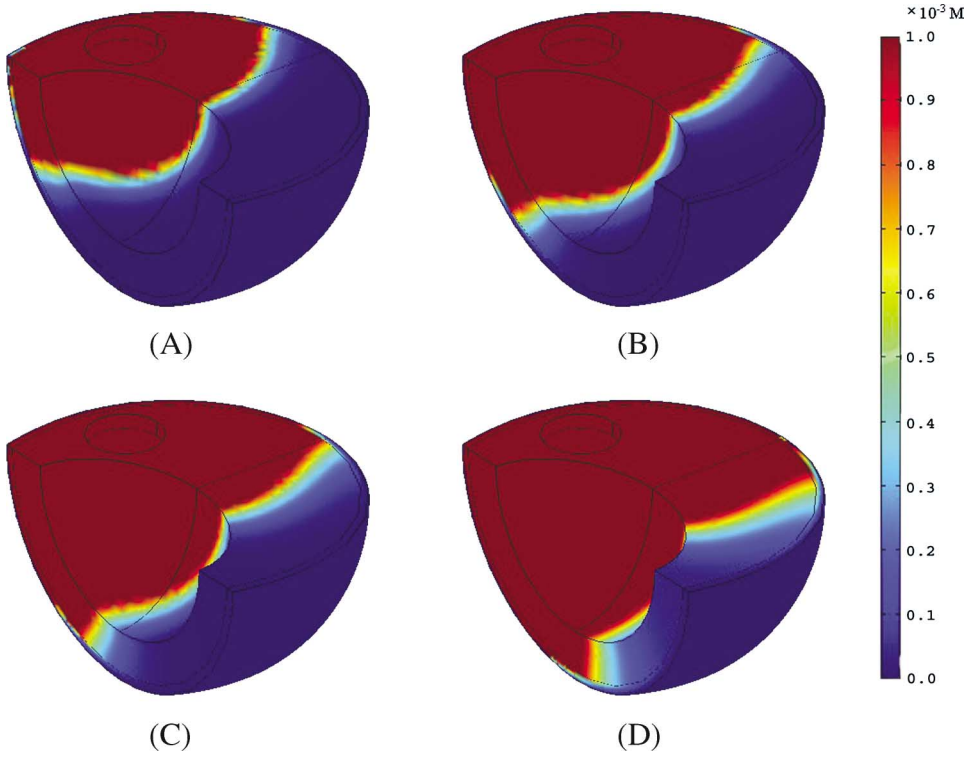

FIGURE 11. Computer simulations of concentration profile contours at various times in the rabbit eye from a release Gd-DTPA implant. Times postimplantation are (1) 1.5 h, (2) 2.68 h, (3) 4.12 h, and (4) 7.67 h.

A more quantitative comparison of the concentration profiles of the MRI image data and the computer simulation is shown in Fig. 12. Here, we see a plot of the normalized Gd-DTPA concentration at one location along a straight line from the lens (0 cm) to the retina surface (0.6 cm) at three time points. MRI experimental data are represented by the points and the simulations are represented by the lines in Fig. 12. There is a reasonable correlation between data and simulation. Notice in the simulations that a concentration gradient can be seen at the retina surface but the concentration profile is flat at the lens surface which is impermeable to Gd-DTPA.

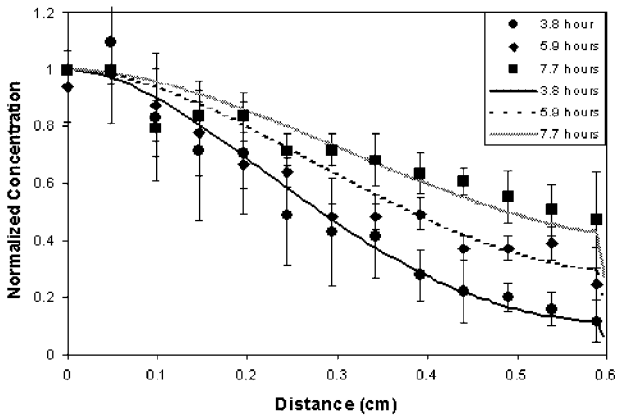

FIGURE 12. Normalized concentration profiles of Gd-DTPA along a horizontal axis from the back of the lens to the retina at various times after PVA implant insertion. Lines are simulation using Gd-DTPA diffusivity in the vitreous of 2.8×10^{-6} cm^2 s^{-1} and diffusivity in the posterior membrane of 6.0×10^{-8} cm^2 s^{-1}.

Some additional theoretical concentration profiles were calculated with the finite element model for the case of the implant releasing according to Fig. 3. These curves are plotted in Figs. 13(A) (*in vivo* case) and 13(B) (*ex vivo* case). These profiles, along a horizontal axis from the back of the lens to the retina, also show a similar qualitative behavior to the MRI images in Figs. 5 and 6, and to the concentration data in Figs. 7(A) (*in vivo*) and 7(B) (*ex vivo*). Actual values may differ due to some variations in the actual *in vitro* release rate. In Fig. 13(A), the concentration increases at the lens surface (0 cm on the *x*-axis) with time and then falls as the release rate from the implant diminishes. At the retina surface (0.65 cm on the *x*-axis), a concentration gradient is always evident. In Fig. 13(B), where the permeability is set to zero to simulate the *ex vivo* case, the concentration profile approaches uniformity over time from the lens to the retina and so, the gradient diminishes.

For didactic purposes, the finite element model was also used to determine several concentration profiles that might occur if steady state conditions were achieved with a continual, constant release device. This situation differs from

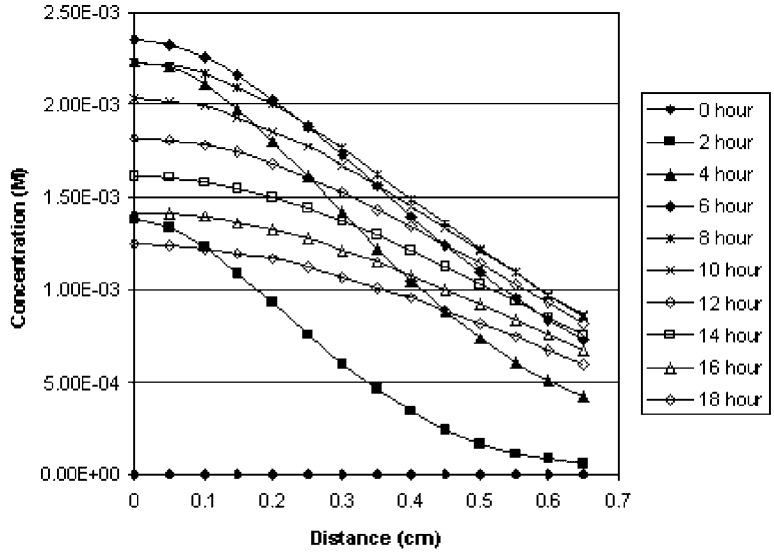

(A)

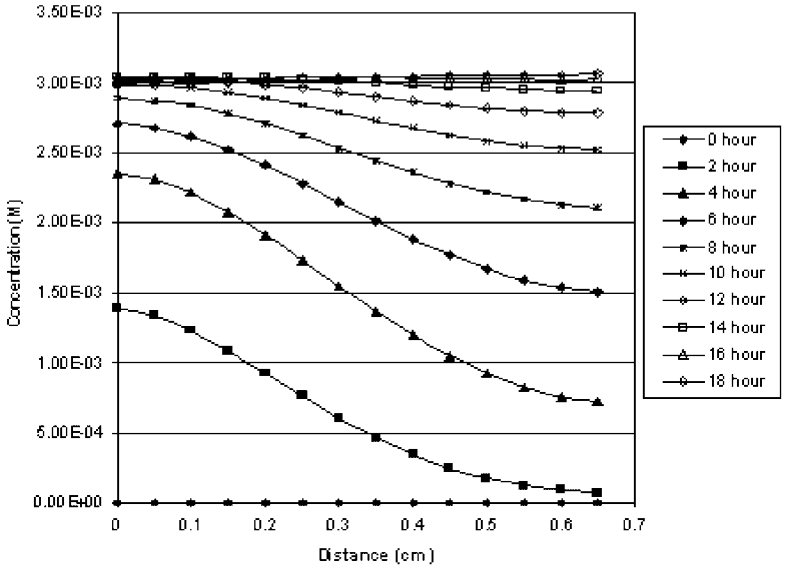

(B)

FIGURE 13. Computer simulation of the concentration profiles along a horizontal axis from the back of the lens to the retina for the PVA implant release: (A) represent the *in vivo* case; (B) represent the *ex vivo* case.

the actual *in vivo* experiments with the Gd implant in that the release rate diminished with time and true steady state could not be achieved. For the hypothetical steady state simulations, a constant release rate of 0.1 mg h^{-1} was used. Figures 14(A) through 14(D) show simulated concentration profiles along an axis from the back of the lens to the retina at different times as predicted by the model for four different values of the posterior membrane permeability coefficients: (A) 10^{-4} cm s^{-1}, (B) 10^{-5} cm s^{-1}, (C) 2×10^{-6} cm s^{-1}(the predicted *in vivo* value), and (D) zero (the presumed *ex vivo* value). At the zero permeability, the concentration gradient at the retina surface has eventually vanished. These simulations give us some idea of when steady state conditions might be achieved for each permeability coefficient. At the highest permeability, steady state concentration profiles are practically achieved by 20 h as seen in Fig. 13(A). By this time, the profile does not appear to be changing with time. Of course, the concentration will continually rise in the vitreous with time for the *ex vivo* case (zero permeability) since the theoretical implant is constantly releasing drug.

Using the hypothetical constant release implant case, computer simulation of concentration profiles along a vertical axis (arrow) are shown in Fig. 15(A) from the implant to the opposite side of the vitreous compartment for a condition representing the *in vivo* permeability case (2×10^{-6} cm s^{-1}), and Fig. 15(B) for the *ex vivo* case

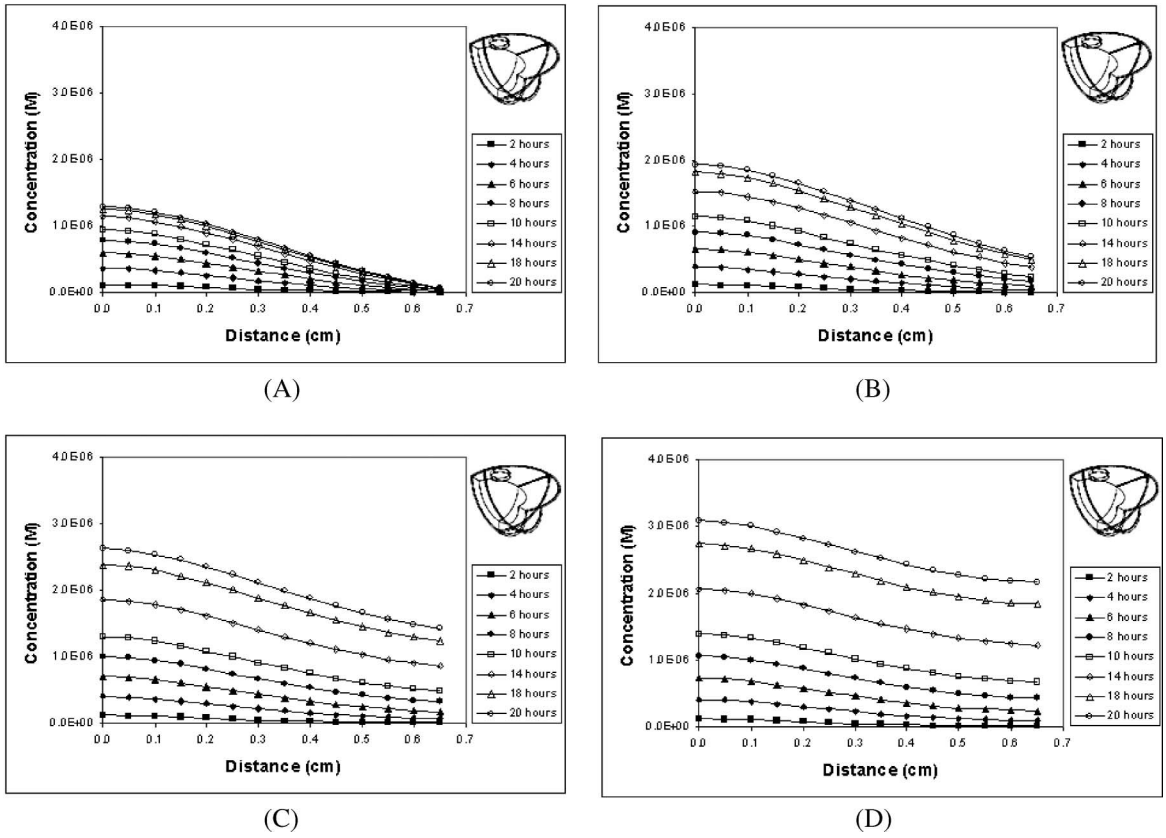

FIGURE 14. Hypothetical concentration profiles for a constant release case of 0.1 mg h^{-1} along a horizontal axis from the back of the lens to the retina at different times predicted by computer simulation for four different values of the posterior membrane permeability coefficients: (A) 1.0 $\times$ 10^{-4} cm s^{-1}, (B) 1.0 $\times$ 10^{-5} cm s^{-1}, (C) 2.0 $\times$ 10^{-6} cm s^{-1}, and (D) 0 cm s^{-1}.

(permeability = zero). Steady state concentrations appear to be approached by about 40 h in the *in vivo* case. However, at 40 h in the *ex vivo* case, concentrations still appear to be rising at a location far from the implant. One would expect the concentration to continue to rise in the *ex vivo* eye (zero permeability) since the implant has constant release rate and there is no exit of drug from the eye.

DISCUSSION

Information on the movement of drugs in the eye is important in determining efficient drug delivery routes, developing new drug delivery methods, and delivering drugs within the desired concentration ranges to the target site with minimal side effects. In this study, we investigated the movement of a small hydrophilic drug surrogate, Gd-DTPA (molecular weight = 958 daltons), released from an implant that was placed in the vitreous cavity of White New Zealand rabbits in both *in vivo* and *ex vivo* experiments. The transport of the Gd-DTPA was monitored by MRI and quantification of Gd-DTPA concentrations over time was obtained. The Gd-DTPA vitreous concentration profiles in rabbit eyes were correlated with a finite element mathematical model of the rabbit eye. Results of the mathematical analyses provided estimates of transport parameters in the rabbit eye such as vitreous diffusion coefficients, and "lumped" posterior membrane permeability (presumably representing the combined retina–choroid–sclera barrier).

Magnetic resonance imaging has proven to be a very useful tool for analyzing drug delivery in the eye. The technique is noninvasive, and gives results in 3D and in pseudo-real time. Lizak *et al.*[25] used a modified fast spin echo sequence technique to image human lenses and was able to detect differences between normal and cataractous eyes. Previous studies reported the use of T_1-weighted MRI imaging for analyzing the diffusion of GD-DTPA through PVA hydrogels[18] and for measuring bioreactor perfusion.[38] These studies analyzed MRI experimental data quantitatively with the relationship between T_1 relaxed values and concentration using inversion recovery MR imaging technique. Kolodny *et al.*[22,23] used MRI to study the eye. They concluded that plasma-derived proteins bypass the posterior chamber of the eye and enter the anterior chamber directly via the iris root. Their analysis was based on MRI images following intravenously injected Gd-DTPA and not specific proteins.

Several studies used contrast enhanced MRI to investigate the breakdown of the blood–retinal barrier created by

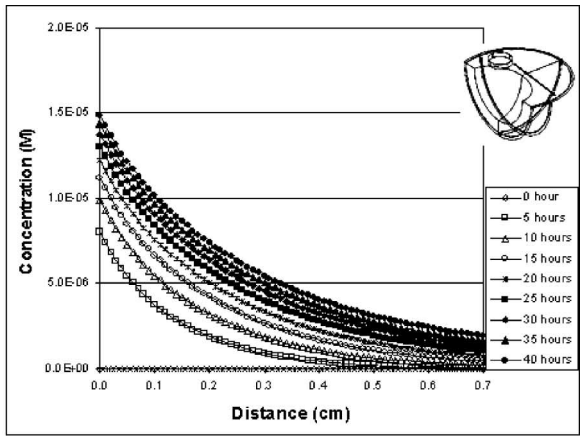

(A)

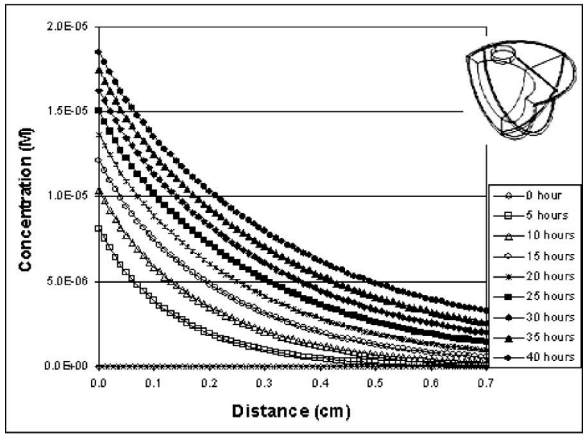

(B)

FIGURE 15. Hypothetical concentration profiles for a constant release case of 0.1 mg h^{-1} along a vertical axis away from the implant at different times predicted by computer simulation for (A) *in vivo* case and (B) *ex vivo* case.

chemical induction or by photocoagulation.[3,4,35] Berkowitz *et al.*[3] produced panretinal photocoagulation in pigmented rabbits and reported a "leakiness" parameter to describe the increase in the permeability of the retina by comparing brightness of Gd-DTPA images from the vitreous. Berkowitz *et al.*[4] and Sen *et al.*[35] used contrast enhanced MRI to study the chemically induced breakdown of two separate components of the blood–retinal barrier: the outer barrier composed of the retinal pigment epithelial cells (RPE) and the inner barrier consisting of the retinal vascular endothelial cells. From their results, they calculated a "modified" permeability-area parameter and they concluded that the RPE disruption resulted in a greater increase in retinal permeability than vascular disruption.

Our diffusion coefficient value for Gd-DTPA in the vitreous compartment was 2.8×10^{-6} cm^2 s^{-1}. This value compares to a free aqueous diffusion coefficient of 3.8×10^{-6} cm^2 s^{-1} as calculated by the Stokes–Einstein equation for a sphere[18] and 2.7×10^{-6} cm^2 s^{-1} calculated by the Wilke–Chang empirical theory using a specific volume of 0.77 ml mg^{-1}.[8] The vitreous is a porous medium composed of approximately 99% (w/w) water and 1% collagen fibers.[12] The proximity of the model vitreous diffusion coefficient with those estimated from free diffusion theory would suggest that the collagen matrix provides minimal hindrance to diffusion of the relatively small molecular weight Gd-DTPA.

The previous reports in the literature of image enhanced MRI studies of the eye were done with intravenous injections of Gd-DTPA. To our knowledge, our study is the first quantitative report of transport in the eye for compounds delivered by intravitreal implants, containing both MRI data and mathematical analysis. We agree with the assertion of Berkowitz[4] that transport of Gd-DTPA is probably by passive diffusion and not active transport.

Other mathematical simulations of drug delivery to the eye have been published. Ohtori and Tojo[30] reported a computer simulation of drug delivery to the eye from intravitreal injections using dexamethasone sodium *m*-sulfobenzoate (DMSB) as the model drug. They concluded that the major route of elimination was via the posterior aqueous humor, especially for hydrophilic drugs, but that the RCS membrane, because of its large area, cannot be overlooked, especially for lipophilic drugs. Tojo and Isowaki[39] presented a pharmacokinetic model for intravitreal drug delivery based on an analysis of diffusion in a cylindrical vitreous body model. They modeled source terms for drug delivery that mimicked reservoir-type and matrix-type release of ganciclovir and the release of DMSB from biodegradable polymer rods. They showed good agreement between average vitreous concentration data and model simulations but their study did not include spatial determination of drug concentration. Freidrich *et al.*[13] presented a sophisticated finite element model of the rabbit eye. Their analysis included fluorescein transport, which is highly permeable through the retina and fluorescein glucuronide transport, which poorly permeates the retina. Examination of the fluorescein simulations shows significant concentration gradients normal to the retinal surface, but for fluorescein glucoronide, these gradients are absent, showing instead concentration contours lines that are perpendicular to the retina. Their simulations are in agreement with the data of Araie and Maurice,[1] and also reflect the findings of our Gd-DTPA MRI data and simulations for the *in vivo* and *ex vivo* experiments. That is to say, for our *in vivo* experiment, the Gd-DTPA is apparently permeable through the RCS layer and shows a sustained concentration gradient from the implant toward the retinal surface. In our *ex vivo* experiments, there is no permeation of the GD-DTPA through the RCS layer and this results in the loss of a concentration gradient toward the retinal surface.

None of the previous models discussed above include convective flow through the vitreous compartment. Stay *et al.*[37] however, have published a computer model of convective and diffusive transport in eyes of humans and

mice. They also include a source term, which is comprised of drug release from a point source made of biodegradable nanoparticles. They concluded that convection plays only a small role for small molecules, but that it may be more important for larger molecules. The relative importance of convection and diffusion in vitreal drug movement is receiving more attention in drug transport studies in the eye. Our model also includes convection velocities in the vitreous, which were calculated from normal intraocular pressures at the hyaloid membrane (15 mm Hg). The fluid velocities vary somewhat as one traverses from the hyaloid membrane toward the posterior segments of the vitreous near the retina since there is an expanding cross-sectional area for flow. A nominal velocity for flow through the RCS barrier in our model is 3.5×10^{-7} cm s^{-1}. This compares favorably with a value reported by Araie and Maurice[1] of 3.9×10^{-7} cm s^{-1} and 3.5×10^{-7} cm s^{-1} by Missel,[28] and 4.0×10^{-7} by Stay[21] and other measures of water flow in the vitreous.[15,27] Missel and Stay both concluded that hydraulic flow is not likely to be of clinical significance for movement of low molecular weight drugs, especially if they are efficiently cleared by the choroid. Likewise, our computer simulations show that reducing the convective flow to zero in the model produces insignificant changes in the Gd-DTPA concentration profiles within the vitreous, suggesting that diffusion is the dominant mechanism for transport in our system. Xu *et al.*[43] calculated Peclet numbers to be 0.4 for a human eye and 0.024 for a mouse eye. The Peclet number reflects the relative importance of flow versus diffusion in transport. Using a nominal velocity at the retinal surface of 3.5×10^{-7} cm s^{-1}, a diffusion coefficient of 2.8×10^{-6} cm^2 s^{-1} in the vitreous, and a nominal length scale of 1.0 cm for the diameter of the vitreous cavity of a rabbit eye, we calculate a Peclet number (vL/D) of approximately 0.09 which implies a dominance of diffusion over flow in affecting the concentration distribution of the Gd-DTPA in the vitreous. Xu's velocity estimate for the Peclet number was based on a Darcy's Law calculation using the combined resistance to flow calculated from the vitreous and scleral hydraulic conductivities, but not including any contribution to flow resistance from the retinal or choroidal layer. They obtained a velocity value of 1.0×10^{-6} cm s^{-1} which is about three times faster than our model value and the values reported by Missel.[28] In any event, the finite element model suggests that Gd-DTPA is eliminated predominately through the RCS barrier.

Other techniques are available for transport studies in eye tissue, such as fluorescein labeling and autoradiography, but these procedures have limitations such as being one-dimensional, requiring animal sacrifice followed by serial sectioning at various time points, and in some cases, being difficult to quantify. Microdialysis has also been reported for analysis of vitreous drug concentrations in the eye.[26]

One potential drawback to the MRI method is the limited availability of actual drug compounds with paramagnetic properties detectable by MRI. Gd-DTPA (gadolinium diethylenetriaminepentaaceticacid) is a water soluble MRI contrast agent with a molecular weight of approximately 938 daltons. It was selected because its molecular weight is similar to drugs of interest in ophthalmologic delivery; it is water soluble; and it is a standard pharmaceutical agent which is FDA approved for use in animals and humans. New compounds are becoming available that are MRI contrast enhancing through chemical conjugation of paramagnetic substances, including a series of high molecular compounds.[5]

We have shown that intravitreal implants can distribute drug throughout the vitreous compartment. However, even at presumed steady state conditions following prolonged delivery, substantial concentration gradients can exits across the vitreal space depending on the positioning of the implant. For diseases that are more dispersed throughout the eye, for example around the entire retina, it is important to take these concentration differences into account in predicting the efficacy of a single positional implant.

Sustained release implant devices can afford opportunities for improving drug delivery in treating chronic eye diseases. The current study has given some insights into the transport processes responsible for disposition of drugs through the vitreous to other ocular regions, like the retina. Mathematical models of ocular drug delivery provide a didactic tool to quantitate transport parameters like vitreal diffusion coefficients and posterior membrane permeabilities and thereby allow more formalized predictions of drug delivery and potential efficacy of new devices and new treatment regimens.

ACKNOWLEDGMENTS

The veterinary technical expertise of Mark Szarowicz and Chris Hillman is gratefully acknowledged.

REFERENCES

[1] Araie, M., and D. M. Maurice. The loss of fluorescein, fluorescein glucuronide and fluorescein isothiocyanate dextran from the vitreous by the anterior and retinal pathways. *Exp. Eye Res.* 52:27–39, 1991.

[2] Avitabile, T., F. Marano, F. Castiglione, C. Bucolo, M. Cro, L. Ambrosio, C. Ferrauto, and A. Reibaldi. Biocompatibility and biodegradation of intravitreal hyaluronan implants in rabbits. *Biomaterials* 22:195–200, 2001.

[3] Berkowitz, B. A., Y. Sato, C. A. Wilson, and E. de Juan. Blood–retinal barrier breakdown investigated by real-time magnetic resonance imaging after gadolinium-diethylenetriaminepentaacetic acid injection. *Invest. Ophthalmol. Vis. Sci.* 32:2854–2860, 1991.

[4] Berkowitz, B. A., P. S. Tofts, H. A. Sen, N. Ando, and E. de Juan Jr. Accurate and precise measurement of blood-retinal barrier breakdown using dynamic Gd-DTPA MRI. *Invest. Ophthalmol. Vis. Sci.* 33:3500–3506, 1992.

[5] Bogdanov, A. A., Jr., R. Weissleder, H. W. Frank, A. V. Bogdanova, N. Nossif, B. K. Schaffer, E. Tsai, M. I. Papisov, and T. J. Brady. A new macromolecule as a contrast agent for

MR angiography: Preparation, properties, and animal studies. *Radiology* 187:701–706, 1993.
[6]Bourlais, C. L., L. Acar, H. Zia, P. A. Sado, T. Needham, and R. Leverge. Ophthalmic drug delivery systems—recent advances. *Prog. Retin. Eye Res.* 17:33–58, 1998.
[7]Cheng, H. M., K. K. Kwong, J. Xiong, and B. T. Woods. Visualization of water movement in the living rabbit eye. *Graefes Arch. Clin. Exp. Ophthalmol.* 230:62–65, 1992.
[8]Cussler, E. L. *Diffusion: Mass Transfer in Fluid Systems*, 2nd ed. New York: Cambridge University Press, 1997.
[9]Dhillon, B., A. Kamal, and C. Leen. Intravitreal sustained-release ganciclovir implantation to control cytomegalovirus retinitis in AIDS. *Int. J. STD AIDS* 9:227–230, 1998.
[10]Duvvuri, S., S. Majumdar, and A. K. Mitra. Drug delivery to the retina: Challenges and opportunities. *Expert Opin. Biol. Ther.* 3:45–56, 2003.
[11]Enyedi, L. B., P. A. Pearson, P. Ashton, and G. J. Jaffe. An intravitreal device providing sustained release of cyclosporine and dexamethasone. *Curr. Eye Res.* 15:549–557, 1996.
[12]Fatt, I. Flow and diffusion in the vitreous body of the eye. *Bull. Math. Biol.* 37:85–90, 1975.
[13]Friedrich, S., Y. L. Cheng, and B. Saville. Finite element modeling of drug distribution in the vitreous humor of the rabbit eye. *Ann. Biomed. Eng.* 25:303–314, 1997.
[14]Funk, R. H., J. Gehr, and J. W. Rohen. Short-term hemodynamic changes in episcleral arteriovenous anastomoses correlate with venous pressure and IOP changes in the albino rabbit. *Curr. Eye Res.* 15:87–93, 1996.
[15]Gaul, G. R., and R. F. Brubaker. Measurement of aqueous flow in rabbits with corneal and vitreous depots of fluorescent dye. *Invest. Ophthalmol. Vis. Sci.* 27:1331–1335, 1986.
[16]Geroski, D. H., and H. F. Edelhauser. Drug delivery for posterior segment eye disease. *Invest. Ophthalmol. Vis. Sci.* 41:961–964, 2000.
[17]Gomori, J. M., R. I. Grossman, J. A. Shields, J. J. Augsburger, P. M. Joseph, and D. DeSimeone. Ocular MR imaging and spectroscopy: An *ex vivo* study. *Radiology* 160:201–205, 1986.
[18]Gordon, M. J., K. C. Chu, A. Margaritis, A. J. Martin, C. R. Ethier, and B. K. Rutt. Measurement of Gd-DTPA diffusion through PVA hydrogel using a novel magnetic resonance imaging method. *Biotechnol. Bioeng.* 65:459–467, 1999.
[19]Huang, X., and C. S. Brazel. On the importance and mechanisms of burst release in matrix-controlled drug delivery systems. *J. Control Release* 73:121–136, 2001.
[20]Hughes, A. A schematic eye for the rabbit. *Vision Res.* 12:123–138, 1972.
[21]Jonas, J. B., I. Kreissig, A. Sofker, and R. F. Degenring. Intravitreal injection of triamcinolone for diffuse diabetic macular edema. *Arch. Ophthalmol.* 121:57–61, 2003.
[22]Kolodny, N. H., T. F. Freddo, B. A. Lawrence, C. Suarez, and S. P. Bartels. Contrast-enhanced magnetic resonance imaging confirmation of an anterior protein pathway in normal rabbit eyes. *Invest. Ophthalmol. Vis. Sci.* 37:1602–1607, 1996.
[23]Kolodny, N. H., S. T. Goode, W. Ryan, and T. F. Freddo. Evaluation of therapeutic effectiveness using MR imaging in a rabbit model of anterior uveitis. *Exp. Eye Res.* 74:483–491, 2002.
[24]Lim, J. I., R. A. Wolitz, A. H. Dowling, H. R. Bloom, A. R. Irvine, and D. M. Schwartz. Visual and anatomic outcomes associated with posterior segment complications after ganciclovir implant procedures in patients with AIDS and cytomegalovirus retinitis. *Am. J. Ophthalmol.* 127:288–293, 1999.
[25]Lizak, M. J., M. B. Datiles, A. H. Aletras, P. F. Kador, and R. S. Balaban. MRI of the human eye using magnetization transfer contrast enhancement. *Invest. Ophthalmol. Vis. Sci.* 41:3878–3881, 2000.
[26]Macha, S., and A. K. Mitra. Ocular pharmacokinetics in rabbits using a novel dual probe microdyalysis technique. *Exp. Eye Res.* 72:289–299, 2001.
[27]Maurice, D. M. Flow of water between aqueous and vitreous compartments in the rabbit eye. *Am. J. Physiol.* 252:F104–F108, 1987.
[28]Missel, P. J. Hydraulic flow and vascular clearance influences on intravitreal drug delivery. *Pharm. Res.* 19:1636–1647, 2002.
[29]Missel, P. J. Finite and infinitesimal representation of vasculature: Ocular drug clearance by vascular and hydraulic effects. *Ann. Biomed. Eng.* 30:1128–1134, 2002.
[30]Ohtori, A., and K. Tojo. *In vivo/in vitro* correlation of intravitreal delivery of drugs with the help of computer simulation. *Biol. Pharm. Bull.* 17:283–290, 1994.
[31]Okabe, J., H. Kimura, N. Kunou, K. Okabe, A. Kato, and Y. Ogura. Biodegradable intrascleral implant for sustained intraocular delivery of betamethasone phosphate. *Invest. Ophthalmol. Vis. Sci.* 44:740–744, 2003.
[32]Pflugfelder, S. C., E. Hernandez, S. J. Fliesler, J. Alvarez, M. E. Pflugfelder, and R. K. Forster. Intravitreal vancomycin. Retinal toxicity, clearance, and interaction with gentamicin. *Arch. Ophthalmol.* 105:831–837, 1987.
[33]Rainer G., R. Menapace, O. Findl, B. Kiss, V. Petternel, M. Georgopoulos, and B. Schneider. Intraocular pressure rise small incision cataract surgery: Randomized intra-individual comparison of two dispersive viscoelastic agents. *Br. J. Ophthalmol.* 85(2):139–142, 2001.
[34]Robinson, M. R., J. Baffi, P. Yuan, C. Sung, G. Byrnes, T. A. Cox, and K. G. Csaky. Safety and pharmacokinetics of intravitreal 2-methoxyestradiol implants in normal rabbit and pharmacodynamics in a rat model of choroidal neovascularization. *Exp. Eye Res.* 74:309–317, 2002.
[35]Sen, H. A., B. A. Berkowitz, N. Ando, and E. de Juan Jr. *In vivo* imaging of breakdown of the inner and outer blood-retinal barriers. *Invest. Ophthalmol. Vis. Sci.* 33:3507–3512, 1992.
[36]Shane, T. S., and D. F. Martin. Endophthalmitis after ganciclovir implant in patients with AIDS and cytomegalovirus retinitis. *Am. J. Ophthalmol.* 136:649–654, 2003.
[37]Stay, M. S., J. Xu, T. W. Randolph, and V. H. Barocas. Computer simulation of convective and diffusive transport of controlled-release drugs in the vitreous humor. *Pharm. Res.* 20:96–102, 2003.
[38]Thelwall, P. E., A. A. Neves, and K. M. Brindle. Measurement of bioreactor perfusion using dynamic contrast agent-enhanced magnetic resonance imaging. *Biotechnol. Bioeng.* 75:682–690, 2001.
[39]Tojo, K., and A. Isowaki. Pharmacokinetic model for *in vivo/in vitro* correlation of intravitreal drug delivery. *Adv. Drug Deliv. Rev.* 52:17–24, 2001.
[40]Tojo, K. J., and A. Ohtori. Pharmacokinetic model of intravitreal drug injection. *Math. Biosci.* 123:59–75, 1994.
[41]Tojo, K., K. Nakagawa, Y. Morita, and A. Ohtori. A pharmacokinetic model of intravitreal delivery of ganciclovir. *Eur. J. Pharm. Biopharm.* 47:99–104, 1999.
[42]Velez, G., and S. M. Whitcup. New developments in sustained release drug delivery for the treatment of intraocular disease. *Br. J. Ophthalmol.* 83:1225–1229, 1999.
[43]Xu, J., J. J. Heys, V. H. Barocas, and T. W. Randolph. Permeability and diffusion in vitreous humor: Implications for drug delivery. *Pharm. Res.* 17:664–669, 2000.
[44]Yamamoto, N., T. Wakabayashi, K. Murakami, and S. Hommura. Detection of CMV DNA in the aqueous humor of AIDS patients with CMV retinitis by AMPLICOR CMV test. *Ophthalmologica* 217:45–48, 2003.